# Mechanochemical Preparation of Novel Polysaccharide-Supported $Nb_2O_5$ Catalysts

**Esther Rincon [1], Araceli Garcia [1], Antonio A. Romero [1], Luis Serrano [2], Rafael Luque [1,3,*] and Alina M. Balu [1,*]**

[1] Departamento de Quimica Organica, Universidad de Cordoba, Campus de Rabanales, Edificio Marie Curie (C-3), Ctra Nnal IV-A, Km. 396, E-14014 Cordoba, Spain; b32rirue@uco.es (E.R.); qo2ganua@uco.es (A.G.); qo1rorea@uco.es (A.A.R.)

[2] Chemical Engineering Department, Faculty of Sciences, Building Marie-Curie, Campus of Rabanales, University of Cordoba, 14014 Cordoba, Spain; iq3secal@uco.es

[3] Scientific Center for Molecular Design and Synthesis of Innovative Compounds for the Medical Industry, People´s Friendship University of Russia (RUDN University), 6 Miklukho-Maklaya str., 117198 Moscow, Russia

* Correspondence: rafael.luque@uco.es (R.L.); qo2balua@uco.es (A.M.B.)

check for updates

**Abstract:** Polysaccharides extracted from natural sources can be used as starting material for the preparation of nanoparticle supported composites. A novel family of bio-nanocomposites was mechanochemically synthesized by using niobium oxide and enzymatically produced polysaccharides. The structural, textural and surface properties of nanomaterials, were determined by X-Ray diffraction (XRD), nitrogen adsorption-desorption (N_2 porosimetry), pulse chromatography, infrared spectroscopy (ATR-IR) and dynamic light scattering (DLS). Selective oxidation of isoeugenol to vanillin was carried out to demonstrate the catalytic activity of the Nb-polysaccharides nanocomposites. Interestingly, most of our material showed high conversion of isoeugenol (60–70%) with selectivity to vanillin over 40%. The optimum conversion and selectivity were achieved with a reaction time between 8 and 24 h.

**Keywords:** mechanochemistry; nanomaterials; polysaccharides; isoeugenol conversion; vanillin production

## 1. Introduction

The most important challenge currently faced by chemistry and related industries is the change towards a more environmentally friendly chemistry. Consequently, it results mandatory understand the efficiency of a process in terms of the replacement of fossil resources by renewable raw materials. In other words, it is necessary to avoid the use of toxic and / or hazardous substances and to eliminate wastes and effluents [1]. In this sense, it is important to focus research on novel green catalytic alternatives because catalysis plays a key role in the cleaner production of chemicals and materials.

In recent years, one of the most important advances in chemistry at both academic and industrial levels has been the use of recyclable catalysts for sustainable and practical chemistry [2–4]. Probably the most efficient strategy has been the heterogenization of highly active catalysts on different organic or inorganic supports [5]. This has achieved the development of significant progress for the effective recovery of the catalyst. Heterogeneous catalysts present great advantages compared to the use of homogeneous phase catalysts. The main one is the ease of separation and recovery of a heterogeneous catalyst. With the development of new heterogeneous catalysts, more efficient processes and methodologies are sought, considering economic and environmental concerns as well as the better

activity and selectivity of the catalysts [3,6–8]. Heterogeneous catalysis can therefore be considered a key and priority activity for a Sustainable Chemistry [9].

On the other hand, nanotechnology has generated a great scientific interest since allows discovering a multitude of new materials. But also evaluating already known materials from a new point of view. This is the case of metallic nanoparticles. They have been known since antiquity and from which, as early as 1857, Faraday [10] performed a first systematic study, based on the synthesis and properties of colloidal suspensions in catalysis [11]. However, it has been in recent years that most progress has been made in this regard.

Nanoparticles (NP) have been studied in recent years due to their high activity, interaction specificity and interesting properties compared to metals (high surface/volume ratio combined with their small sizes) [12–14]. The specific properties of NP are directly related to their morphology and size, the dispersion of the metal or metal oxide on the support, the metal loading and the electronic properties of the NP in the material. In addition, NP have the additional advantage of their recyclability and reuse. These are essential and desired properties in many applications of these nanomaterials in catalysis [12,15], sensors [15,16] and even in the field of medicine [12]. There are several methods for the preparation of NP. Some of them include conventional physic-chemical methodologies of impregnation/reduction and coprecipitation [13,15,17], precipitation/deposition [13,15,17,18]. Nowadays more innovating methods have appeared such as photochemical deposition [13,15,17], ultrasonic deposition [13,15,17,18], use of laser treatment [13,15,17], supercritical fluids [13,15,17,19], plasma [13,15,17] or microwave irradiation [13,15,17,20,21].

The mechanochemistry is a novel procedure for the production of NP. It consists on the melting, deformation and fracture of a mixture of reactants, normally solid, in a repetitive way during grinding. This reaction takes place at the interface of nanosized particles, those which are being continuously formed. Therefore, the process does not require any external heat input as the case of conventional chemical reactions. The process mechanism, is not yet clear due to the diversity of reaction types, conditions and materials used. The are some factors that hinders the advanced knowledge and progress of this type of processes with clarity. Some of them are the heterogeneous nature of solid-solid reactions, the difficulty in observing directly the materials that are undergoing the mechanochemical process at the microscopic or molecular level and the lack of study of some types of reactions [18]. This procedure has a potential applicability not only due to [18] the high acceptance, effectiveness and reproducibility of this procedure in any type of synthesis but also the possibility of not using solvents in the process, avoiding the environmental problems and toxicity related to the use of them. These characteristics make mechanochemical milling a very attractive nanocatalysts synthesis technique. In addition, the required synthesis time is much shorter than in other synthesis techniques such as hydrothermal treatment [22]. There are several examples that have demonstrated the great potential of these mechanochemically synthesized NP. Recently, our research group has prepared different types of metal NP and metal oxides that have different applications in heterogeneous catalysis processes [18,21,23,24].

On the other hand, nature has inspired scientists to innovate and design novel materials. Polysaccharides offer a real alternative to synthetic polymers in the preparation of soft nanomaterials. They have also been used in composite materials with hard nanomaterials, such as metal nanoparticles and carbon-based nanomaterials [25]. Natural polysaccharides have been used for many years as supports for enzymatic catalysts. They recently received attention as supports for metal catalysts. The advantages of using polysaccharides are their high natural availability and renewable character, their high functionality that make them easily linkable to metals, good physical and chemical versatility, insolubility in most of organic solvents and their complex structure, providing interesting textural properties to the so templated catalysts [26]. Previous studies have reported the good performance of these carbohydrates-supported catalysts [27,28] for novel green catalysis processes.

Vanillin (4-hydroxy-3-methoxybenzaldehyde) is found in nature in vanilla plant extract (*Vanilla planifolia*), as well as roasted coffee (*Coffea spp.*) and Chinese red pine (*Pinus massoniana*). This

compound is widely used as a medical flavouring additive (in the production of pharmaceuticals and to mask unpleasant drug odours) and in food, beverage and perfume industry (for example, in the production of ice cream, sweets and chocolates). The annual worldwide demand for vanillin is 12000 tonnes, being only 1800 tonnes are produced from natural sources [29]. Vanillin can be biotechnologically prepared from eugenol (4-allyl-methoxyphenol) or isoeugenol (2-methoxy-4-(prop-1-en-1-yl) phenol) or by chemical synthesis [30]. Essentials oils from spices represent economical substrates for natural eugenol and isoeugenol as intermediates for vanillin production [31]. Besides, isoeugenol can be produced synthetically by thermal or chemical isomerization of eugenol and the reaction of phenylmagnesium bromide with isosafrole [32].

A method for the catalytic oxidation of isoeugenol to vanillin has been described using $H_2O_2$ as oxidant agent [33]. However, this reaction requires the use of quite expensive catalysts (methyltrioxorene) [27] and of anhydrous $H_2O_2$. Therefore, the development of new economic and efficient catalysts for these conversions is required. A system based on niobium oxide (low cost chemical) and polysaccharides (renewable, sustainable and low-cost production) using mechanochemistry (without solvent) could be more economical.

Based on these premises, the present study proposes the synthesis of Nb nanomaterials by means of mechanochemical processes using a series of biopolymers (polysaccharides) as sacrificial templating agents. These novel nanomaterials were subsequently evaluated as catalysts to produce vanillin from isoeugenol.

## 2. Results

Nb$_2$O$_5$-polysaccharides catalysts were synthesized using mechanochemistry. Mechanochemical milling provides a powerful technique for minimizing the use of hazardous solvents. Moreover, our system used polysaccharides, as sacrificial templating agents, those which could be obtained from agricultural wastes. Thereby, the present study contributes to minimize the impact on the environment according to the green chemistry principles. The synthesized nanocatalysts incorporate Nb$_2$O$_5$ and different exopolysaccharides (called S4, S7, S12, S13 and S14). The new as obtained materials were labelled as S14-Nb$_2$O$_5$, S7-Nb$_2$O$_5$, S12-Nb$_2$O$_5$, S13-Nb$_2$O$_5$ and S14-Nb$_2$O$_5$.

### 2.1. Infrared Spectroscopy Analysis

In Figure 1 the infrared spectra of the used exopolysaccharides and Nb nanocomposites are shown. As observed in Figure 1a all the starting samples showed typical absorption bands related to polysaccharides. The broad peak at 3300 cm$^{-1}$ is assigned to –OH groups and those around 2940 and 2850 cm$^{-1}$ attributed to the asymmetric C–H stretching of CH$_2$ and CH$_3$ moieties [28]. Two prominent peaks appear at around 1640 and 1535 cm$^{-1}$, related with amide I and amide II species, indicating the presence of proteins [34] and a band found at 1040 cm$^{-1}$ attributed to the C–O–C contributions in glycosidic linkages, indicating that simples are mainly composed by xylan-type polysaccharides [28]. The peak at 1455 cm$^{-1}$ was attributed to CH$_2$ in polysaccharides, the band at 1310 cm$^{-1}$ to symmetric CH$_2$ bending, the one at 1089 cm$^{-1}$ to C–O stretching of β-glucans and the one at 1013 cm$^{-1}$ to stretching vibration of C–O α-glycosidic bond. The band at 929 cm$^{-1}$ was attributed to β-glycosidic bond; C–O and C–C stretching. Beyond 700 cm$^{-1}$ bands become difficult to assign, mainly arising from hydrogen bonds between hydroxyl side chains in xylan-type structure [34].

A clear difference in the 1650–1500 cm$^{-1}$ and 1100–1000 cm$^{-1}$ regions was noted for the analysed samples. Thus, S4 and S13 exopolysaccharides showed a low intensity of bands above attributed to proteins, indicating that these samples probably deproteinized before being used [34,35]. However, for the S7 polysaccharide the predominant band in this region pointed out a higher content of proteins. On the other hand, in the vibration region related with C–O unit bonding the spectra resulted significantly different. As discussed by Kačuráková et al. [34], a sole strong band around 1040 cm$^{-1}$ indicates that polysaccharide has a predominant β(1-4)xylan backbone, while for β(1-3)-linked xylan two bands around 1070 cm$^{-1}$ and 1030 cm$^{-1}$ appear. This fact would indicate that S13 and S14 samples

have a predominant (1-4)xylan principal structure, S12 and S4 have a mixture of (1-4) and (1-3) bonded xylan skeleton and that S7 sample was mainly composed by a (1-3)xylan-type polysaccharide.
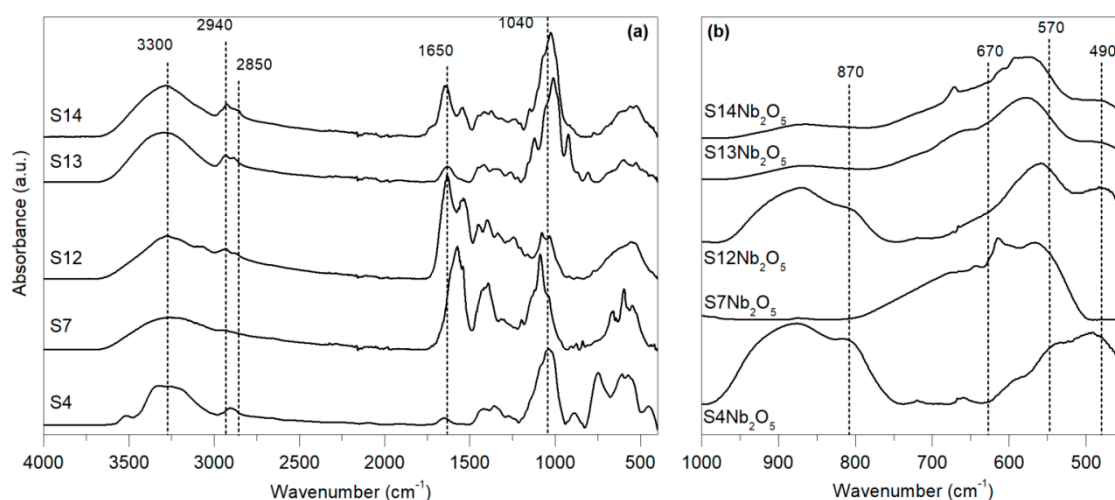


**Figure 1.** ATR-IR spectra of (**a**) exopolysaccharides and (**b**) biotemplated Nb based catalysts.

Figure 1b shows the IR spectra of prepared Nb based catalysts, where the carbonaceous support was removed after calcination [27]. As discussed by Ikeya and Senna [36], peaks from 740 to 580 cm$^{-1}$ are related to Nb-O-Nb bridging compounds. The broad band at 870 cm$^{-1}$ can be assigned to distorted Nb-O-Nb stretching vibrations reported for $NbO_6$ units with pseudohexagonal phase in high crystalline structure [36,37]. This peak clearly appeared in S4-$Nb_2O_5$ and S12-$Nb_2O_5$ samples, suggesting a higher structural arrangement. However, this band was weak for S13-$Nb_2O_5$ an S14-$Nb_2O_5$ materials and almost missing in S7-$Nb_2O_5$ exopolysaccharide, this indicating a different crystalline structure. The evidence differences between samples confirmed the occurrence of a mechanochemical reaction between exopolysaccharides and Nb precursor, in agreement with previous works [38].

### 2.2. Morphology of $Nb_2O_5$-Polysaccharides Based Nanoparticles

XRD diffractograms of the exopolysaccharides used as sacrificial template (S4, S7, S12, S13 and S14) showed the amorphous character of the polysaccharides, except for the S4 sample that presented high crystallinity (data not shown). XRD diffractograms of mechanochemically synthesized Nb nanocomposites are shown in Figure 2. As observed, S4-$Nb_2O_5$ catalyst was the most crystalline sample, with a clear pseudohexagonal structure [39] due to the existence of dominant diffractions peaks at 22.5° (001), 28.3° (180), 36.5° (181), 46.1° (002), 50.5° (380) and 54.8° (212). However, the other prepared catalysts presented polymorphism due to the mixture with other crystalline phases. For instance, S12-$Nb_2O_5$ sample exhibit high crystallinity in a predominant pseudohexagonal structure but with the presence of two peaks at 29.5° and 32.7° related to (311) and (222) planes of a pyrochlore type crystalline structure [40,41]. This phase resulted more evident for S7-$Nb_2O_5$ nanocomposite, being also quite crystalline, whereas S13-$Nb_2O_5$ and S14-$Nb_2O_5$ presented a more amorphous character. These results agree with the above IR analyses that pointed out a clear structural difference on the Nb based composites (Figure 1b).

The presence of different phases in $Nb_2O_5$ samples has been reported to be directly related to the starting materials, the synthesis method and the calcination temperature [40,42]. The formation of pyrochlore type and pseudohexagonal crystalline structures occurs at 300–600 °C, justifying the presence of a mixture of these phases in the prepared samples. Moreover, the clear structural difference observed in IR analyses of starting exopolysaccharides supported this conclusion (Figure 1a). Three-fold helix conformation has been reported for (1-4)linked xylan [34], being found for S13 and S14 samples, whereas the (1-3)-type chains, assigned to S4, S12 and S7 polysaccharides, would form an

entirely different structure with a more arranged triple-stranded helical rope stabilised by hydrogen bonds. These different arrangements clearly influenced the crystallization of niobium oxide during the preparation of the nanocatalysts and therefore affected the polymorphism of the resulting Nb based composites.
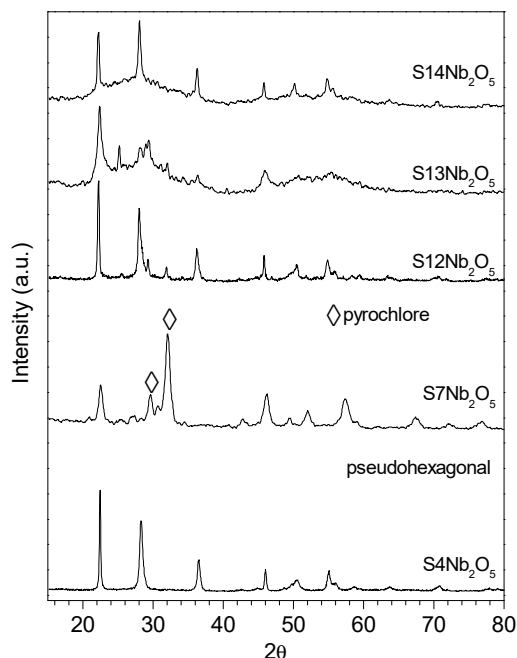


**Figure 2.** XRD patterns of polysaccharide templated Nb based catalysts.

### 2.3. Porosity and Acidity of Biotemplated $Nb_2O_5$ Catalysts

The textural properties of the different synthesized Nb based materials are summarized in Table 1. It can be observed that the synthesized catalysts presented a low porosity, with surface areas between 15 and 45 $m^2\,g^{-1}$. Similar values (between 27 and 48 $m^2\,g^{-1}$) were observed by Murayama et al. [40] for $Nb_2O_5$ based catalysts with pseudohexagonal, pyrochlore and amorphous morphology but resulted higher than those reported by Xu et al. [38] for ZnO-polysaccharide nanohybrids. The porosity observed for these materials resulted as meso-type and macroporous surface, with a significant contribution of interparticular macroporosity in the materials, which explains the high pore volumes obtained in the measurement (between 1.24 and 2.75 $mLg^{-1}$) and that do not correspond to "real" porosity of the material but to the described interparticular porosity.

**Table 1.** Textural and acidic properties of synthesized $Nb_2O_5$-polysaccharide nanohybrids and results of isoeugenol oxidation using prepared catalysts under conventional heating at 90 °C (maximum isoeugenol conversion and vanillin selectivity).

| Material | $S_{BET}$ $(m^2g^{-1})$ [a] | $V_{BJH}$ $(mLg^{-1})$ [b] | $D_{BJH}$ (nm) [c] | PY Acidity [d] $(mmol\,g^{-1})$ | DMPY Acidity [e] $(mmol\,g^{-1})$ | Conversion [f] (%mol) | $S_v$ [g] (%mol) |
|---|---|---|---|---|---|---|---|
| S4-$Nb_2O_5$ | <25 | 1.36 | 12.06 | 0.04 | 0.03 | 62.3 | 51.6 |
| S7-$Nb_2O_5$ | <25 | 1.24 | 10.61 | 0.01 | 0.01 | 24.5 | 12.0 |
| S12-$Nb_2O_5$ | 35 | 1.47 | 84.81 | 0.03 | 0.03 | 62.7 | 60.7 |
| S13-$Nb_2O_5$ | 34 | 2.75 | 16.20 | 0.04 | 0.02 | 70.1 | 53.3 |
| S14-$Nb_2O_5$ | 45 | 1.31 | 57.74 | 0.04 | 0.02 | 55.1 | 48.6 |

[a] $S_{BET}$: specific Surface area was calculated by the Brunauer-Emmett-Teller (BET) equation; [b] $V_{BJH}$: pore volumes were calculated by Barret-Joyner-Halenda (BJH) equation; [c] $D_{BJH}$: mean pore size diameter was calculated by the Barret-Joyner-Halenda (BJH) equation; [d] Total acidity determined by pulse chromatographic method using pyridine; [e] Brönsted acidity determined by pulse chromatographic method using 2,6-dimethylpyridine; [f] maximum conversion values reached after 8 h of reaction; [g] maximum selectivity values reached after 24 h of reaction.

The results of the surface acidic properties for synthesized Nb nanocomposites are also displayed in Table 1. It can be seen that all the catalysts presented acidic centres of both Lewis and Brönsted type. The acidity of all the investigated materials resulted in general quite low compared to other types of acid porous materials such as aluminosilicates of type MCM-41, SBA-15 or microporous zeolites.

## 2.4. Catalytic Activity

The conversion of isoeugenol and vanillin selectivity over the synthesized bio-templated Nb catalysts are shown in Figure 3.
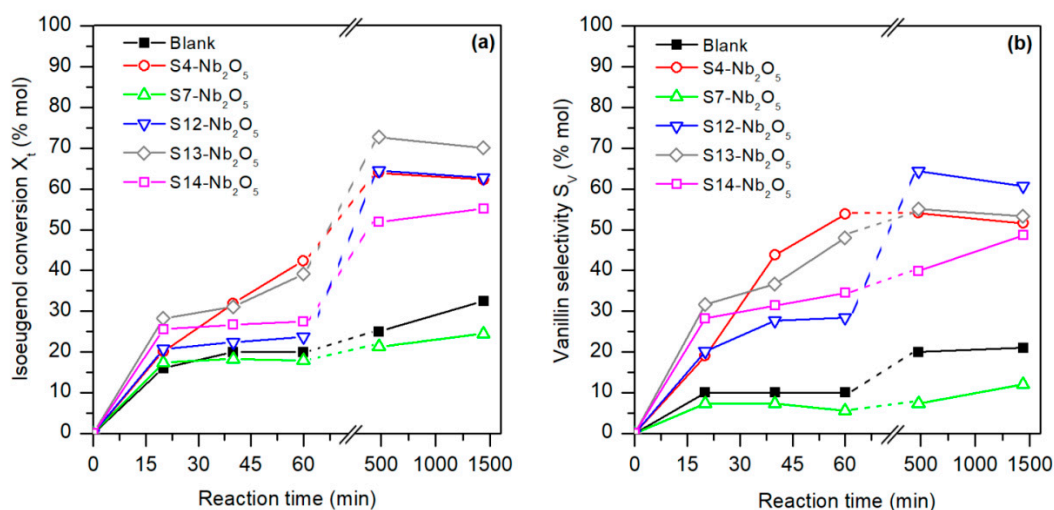


**Figure 3.** Catalytic activity of synthetized Nb/polysaccharide materials as the variation of (**a**) isoeugenol conversion (% mol) and (**b**) vanillin selectivity (% mol) with the reaction time.

Concerning the kinetic study of the catalytic activity in the conversion reaction of isoeugenol into vanillin, the nanocatalysts achieved conversions in the range of 60–70% (Figure 3a), with selectivity to vanillin >40% (Figure 3b) when the reaction ran for more than 8 h, except for $S7-Nb_2O_5$, which showed results even worse than the blank experiment (24.5% conversion and 12.0% selectivity after 24 h).

At short reaction times (less than 3 h), low conversion was observed for all nanocomposites, as well as vanillin selectivity (<30%), except for the $S13-Nb_2O_5$ material that already presented significant conversion and a moderate selectivity to vanillin (about 50%). $S12-Nb_2O_5$ and $S13-Nb_2O_5$ materials exhibited the highest conversion and selectivity to vanillin after 8 h of reaction under the condition studied, reaching values about 65% for $S12-Nb_2O_5$ catalysts. As observed, total isoeugenol conversion and vanillin selectivity reached a maximum after 24 h for $S7-Nb_2O_5$ and $S14-Nb_2O_5$, whereas for $S4-Nb_2O_5$, $S12-Nb_2O_5$, $S13-Nb_2O_5$, better results were obtained after 8 h of reaction, remaining almost constant for longer reaction times.

The high porosity of catalyst facilitates the adsorption/desorption mechanism of reactants and products, making the catalytic process comparably faster to that for nonporous or microporous materials [26]. Thus, the higher and faster isoeugenol conversion observed for $S13-Nb_2O_5$ sample (70.1% mol) would be due to the larger pores (2.75 mLg$^{-1}$) observed on its surface. Moreover, previous works asserted that the catalytic activity as a solid acid and surface area of $Nb_2O_5$ based catalysts decreased with the crystallinity degree [40], being the presence of labile protons on distorted amorphous niobium oxide those regarded as potential active sites in solid acid catalysts for extensive organic reactions [41]. Muruyama et al. [40] also asserted that the alkylation selectivity to benzyl anisole of different niobium oxide nanoparticles resulted higher for pseudohexagonal arrangements, followed by amorphous and pyrochlore type structures. This agrees with the results of the present work, where $S12-Nb_2O_5$, with pseudohexagonal crystalline structure and moderate porosity, reached the higher vanillin selectivity (60.7% mol).

During the conversion of isoeugenol to vanillin, using our $Nb_2O_5$-polysaccharides catalysts, secondary reactions are produced. Compounds such as eugenol, diphenylether and oligomers (calamenene) are generated avoiding the 100% conversion. This may due to the low acidity presented by the catalysts compared to traditional acid catalysts used in the same reaction [22].

Thus, the combination of a moderate acidity of both Brönsted and Lewis types for these materials seems to be related to an optimum activity and selectivity in the studied reaction conditions, although this relationship appears to be rather more complex than just acidity, so further studies are need for their understanding.

## 2.5. Particle size Distribution and Water Stability

Most bio-based catalytic processes take place in aqueous medium. For this reason and to ensure the dispersion and stability of the NP and to avoid their agglomeration, it is important to study the water stability of the catalyst. In order to evaluate the stability of $Nb_2O_5$-polysaccharide based nanoparticles in presence of water, the zeta potential was measured in the pH range 2–12. The suspension of nanoparticles is considered stable at $\pm 25$ mV since it is considered as the value when the repulsion force between particles is enough to not form aggregates [42]. The catalysts with the best catalytic conversion rate (S13-$Nb_2O_5$ and S12-$Nb_2O_5$) showed water stability in pH range 4–12, however, with strong acidic pH, the catalysts present a small electrostatic charge which will result in agglomeration of the NP and thus worsening of the catalytic process.

The particle size of a nanoparticle can affect the performance of the catalyst because of the active sites on the surface of the catalyst. Dynamic Light Scattering was recorded at pH 12 (maximum zeta potential) to ensure the NP dispersion. According to the results of DLS analysis presented in Figure 4 the average hydrodynamic diameter of S12-$Nb_2O_5$ nanoparticles was 189.8 nm and of S13-$Nb_2O_5$ nanoparticles was 150.2 nm.
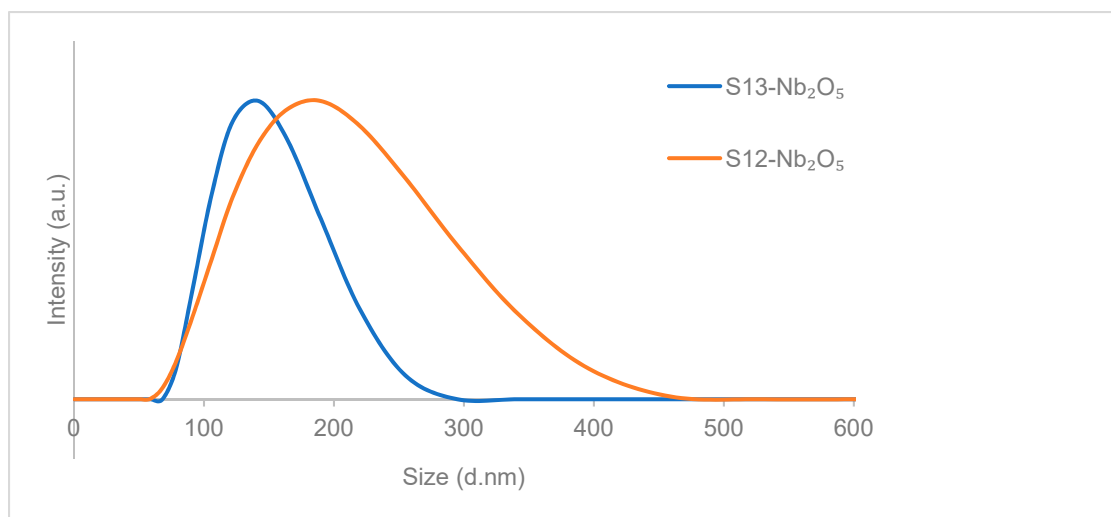


**Figure 4.** Hydrodynamic size distribution of S12-$Nb_2O_5$ and S13-$Nb_2O_5$ nanocatalysts.

## 3. Materials and Methods

### 3.1. Materials

For the preparation of nanomaterials different polysaccharides (exo-polysaccharides) generated by microbial fermentations—named S4, S7, S12, S13 and S14—were used as structure directing agents, gently provided by Heihua Biotechnotic Ltd. (Zhengzhou, China). Niobium salt (Ammonium niobate (V) oxalate hydrate) was used as a metal precursor in order to obtain niobium oxide in the final materials.

For the catalytic activity evaluation, isoeugenol (Sigma Aldrich: 98% purity, Madrid, Spain) as reactant, $H_2O_2$ (Sigma Aldrich: 50% purity) and acetonitrile (Panreac: 99.9% purity, Madrid, Spain) as the solvent were used.

**Synthesis of $Nb_2O_5$-Polysaccharides Nanohybrids:** The synthesis of novel nanomaterials was carried out following a simple, reproducible and environmentally friendly protocol [43]. The five nanocomposites based on a niobium precursor and the polysaccharides (S4, S7, S12, S13 and S14) were obtained by mechanochemical processing in a ball mill (Retsch PM 100 planetary ball mill, Asturias, Spain) with a 25 mL reaction chamber and 8 mm stainless steel ball. For this, different amounts polysaccharides and Nb precursor at 20% *w/w* were used. These mixtures were processed at 350 rpm in a ball mill for 30 min. Subsequently, the materials were kept 24 h at 100 °C and finally calcined at 600 °C for 3 h under air. The obtained materials were labelled according to the type of polysaccharides used as S4-$Nb_2O_5$, S7-$Nb_2O_5$, S12-$Nb_2O_5$, S13-$Nb_2O_5$ and S14-$Nb_2O_5$.

### 3.2. Materials Characterisation

#### 3.2.1. X-ray Diffraction (XRD)

X-ray diffraction technique was used for the structural study of the synthesized nanocomposites. The diffractograms were obtained on a Bruker D8 Discover diffractometer (Madrid, Spain), equipped with a Bragg Brentano θ/θ High Precision Goniometer, a Cu X-ray tube, a rotating platform, a primary beam monochromator and an ultra-high-speed detector. The sweep was performed in the range of $10 < 2\theta < 80$.

#### 3.2.2. ATR-IR

The chemical structure of the polysaccharides and nanocomposites was evaluated by attenuated-total-reflectance infrared spectroscopy (ATR-IR) by direct absorbance in a single-reflection ATR System (ATR top plate fixed to an optical beam condensing unit with ZnSe lens) with an MKII Golden Gate SPECAC instrument (Kent, UK). Spectra were recorded over 20 scans with a resolution of $4\ cm^{-1}$ in a wavelength range between 4000 and $400\ cm^{-1}$ [44].

#### 3.2.3. Porosimetry by Adsorption-Desorption Behaviour ($N_2$ Porosimetry)

Nitrogen adsorption/desorption isotherms were obtained using liquid nitrogen (−196 °C) on a Micrometrics ASAP 2000 analyser (Ottawa Ontario, Canada). The five solids were subjected to a pre-degassing process at a temperature of 100–125 °C for 24 h. Surface areas were calculated according to the linear part of the Brunauer, Emmett and Teller (BET) equation in the range of $0.05 < P_0 < 0.30$. Pore size distribution (PSD) was calculated using the adsorption branch of the nitrogen adsorption-desorption isotherm and the Barret-Joyner-Halenda formula (BJH). The total pore volume, $V_{BJH}$, was obtained from the PSD profiles [45].

#### 3.2.4. Acidic Properties

The pulse chromatographic method was used to study the surface acid properties. In order to determine the surface acidity of the synthesized catalysts, pyridine (PY) and 2,6-dimethylpyridine (DMPY) were chosen as bases for the adsorption of both types of acidic, Brönsted and Lewis centres and on Brönsted acid centres, respectively. The analyses were carried out at 70 °C for the PY and 90 °C for the DMPY assays. The pulses were induced by means of a microinjector in the catalytic bed from a cyclohexane solution of the titrant (0.989 M in PY and 0.500 M in DMPY). The catalyst was standardized prior to each titration in a dehydrated and deoxygenated (99.999% purity) nitrogen (50 mL/min) for 1 h flow rate at 70 °C for the PY titration and 90 °C for the DMPY titration. The catalyst (~0.025 g) was fixed by Pyrex glass wool buffers into a 4 mm flame-ionisation stainless steel tubular microreactor, using an analytical column Chromosorb AW-DMCS 80/100 of 0.5 m in length containing 5% by weight of polyphenylether.

*3.3. Catalytic Activity*

In order to evaluate the catalytic activity of the synthesized materials, the conversion of isoeugenol to vanillin was conducted by a selective oxidative cleavage reaction under conventional heating conditions (conventional liquid phase).

The reaction mixture was analysed by gas chromatography on an Agilent Technologies 7890 A GC System (Madrid, Spain) equipped with a Petrocol™ DH column (100 m × 0.25 mm × 0.50 μm) and a flame ionization detector (FID). The temperature of the column was set at 200 °C (70 min hold time) and the temperature of the injector and detector at 300 °C. The nitrogen gas flow was set at 3 mL min$^{-1}$. Isoeugenol calibration was carried out in the 2.00–60.00 g L$^{-1}$ range (r$^2$ 0.98). The identification and resulting retention time of the products under the above conditions were eugenol (28 min), vanillin (30 min), diphenyl ether (31 min), isoeugenol (33 min) and calamenene oligomers (37 min) [45].

The catalytic reaction in liquid phase with conventional heating was carried out using a multiple parallel synthesis system model Carousel Reaction Station™ (Radleys Discovery Technologies, Essex, UK). The reaction tube, with a volume of about 45 mL, was equipped with magnetic stirring. For the sampling of the medium a syringe was used, taking regular aliquots through a coupled filter to avoid the extraction of the solid catalyst. The reaction conditions used were isoeugenol (0.8 mL/5·10$^{-3}$ mol), hydrogen peroxide (1.2 mL/1.2·10$^{-3}$ mol), acetonitrile (8 mL/152·10$^{-3}$ mol) and 0.1 g of catalyst. The experiment was carried out at 90 °C.

*3.4. Dynamic Light Scattering (DLS) and Zeta Potential*

The zeta potential and size distribution of S12-Nb$_2$O$_5$ and S13-Nb$_2$O$_5$ (catalysts which present the highest catalytic activity) were measured using a Zetasizer (ZSP, Malvern Instrument Ltd., Worcestershire, UK) at 25 °C based on laser Doppler velocimetry and dynamic light scattering techniques. Each sample was prepared at 2 × 10$^{-5}$ g/mL using milli-Q water as solvent and inert electrolyte. Previously, the suspension was homogenized using a ultrasonication probe for a period of 30 s. The refraction index values for the dispersant was set as 1.33 and for the material (Nb$_2$O$_5$) as 2.34. The analysis was realized by triplicate and medium and standard deviation was calculated.

The zeta potential was measured to evaluate the stability in water in the pH range 2–12 using NaOH 0.1 N and HCl 0.1 N.

**4. Conclusions**

In this study, a novel set of Nb-based nanocomposites were prepared by means of a simple, efficient and environmentally friendly mechanochemical dry milling protocol, using a Nb precursor and different exopolysaccharides derived from microbial fermentation. This work was developed using the premise that a system Nb-polysaccharide synthesized by mechanochemistry could provide a low-cost catalytic system with high conversion rates. IR spectra and XRD diffraction patterns demonstrated that the starting polysaccharide used as sacrificial template reacted during the mechanochemical synthesis and, therefore, the crystallization of niobium during calcination step resulted highly affected by the biotemplate structure and composition. Synthesized nanomaterials exhibited low porosity (generally interparticular meso- and macroporosity) as well as low acidity values (both Brönsted and Lewis related measurements). Despite their low acidity as compared to most reported solid acids in literature, the synthesized nanocomposites exhibited a remarkable catalytic activity during the selective oxidation of isoeugenol to vanillin under conventional heating (90 °C). Thus, S12-Nb$_2$O$_5$ and S13-Nb$_2$O$_5$ nanocomposites provided the best values of isoeugenol conversion (60–65%) and vanillin selectivity (55–65%), respectively, making these novel systems highly promising for mild acidic catalysed processes as well as mild selective oxidations.

**Conflicts of Interest:** The authors declare no conflict of interest.

## References

1. Sheldon, R.A. Engineering a more sustainable world through catalysis and green chemistry. *J. R. Soc. Interface* **2016**, *13*, 20160087. [CrossRef]

2. Lu, F.; Ruiz, J.; Astruc, D. Palladium-dodecanethiolate nanoparticles as stable and recyclable catalysts for the Suzuki-Miyaura reaction of aryl halides under ambient conditions. *Tetrahedron Lett.* **2004**, *45*, 9443–9445. [CrossRef]

3. Astruc, D.; Lu, F.; Aranzaes, J.R. Nanoparticles as recyclable catalysts: The frontier between homogeneous and heterogeneous catalysis. *Angew. Chem. Int. Ed.* **2005**, *44*, 7852–7872. [CrossRef] [PubMed]

4. Astruc, D. Transition-metal nanoparticles in catalysis. In *Nanoparticles and Catalysis*; Wiley-VCH: Weinheim, Germany, 2008.

5. Agblevor, F.A.; Jahromi, H. Aqueous phase synthesis of hydrocarbons from reactions of guaiacol and low molecular weight oxygenates. *ChemCatChem* **2018**, *10*, 5201–5214. [CrossRef]

6. White, R.J.; Luque, R.; Budarin, V.L.; Clark, J.H.; Macquarrie, D.J. Supported metal nanoparticles on porous materials. Methods and applications. *Chem. Soc. Rev.* **2009**, *38*, 481–494. [CrossRef] [PubMed]

7. Grunes, J.; Zhu, A.; Somorjai, G.A. Catalysis and nanoscience. *Chem. Commun.* **2003**, *0*, 2257–2260. [CrossRef]

8. Jahromi, H.; Agblevor, F.A. Hydrodeoxygenation of aqueous-phase catalytic pyrolysis oil to liquid hydrocarbons using multifunctional nickel catalyst. *Ind. Eng. Chem. Res.* **2018**, *57*, 13257–13268. [CrossRef]

9. Anastas, P.; Warner, J. *Green Chemistry: Theory and Practice*; Oxford University Press: New York, NY, USA, 1998.

10. Faraday, M. Experimental Relations of Gold (and other Metals) to Light. *Philos. Trans. R. Soc. Lond.* **1857**, *147*, 145–181.

11. Braunstein, P. *Metal Clusters in Chemistry*; Wiley-VCH: Weinheim, Germany, 1999.

12. Polshettiwar, V.; Varma, R.S. Green chemistry by nano-catalysis. *Green Chem.* **2010**, *12*, 743–754. [CrossRef]

13. Ozin, G.A.; Arsenault, A.; Cademartiri, L. *Nanochemistry: A Chemical Approach to Nanomaterials*, 2nd ed.; Royal Society of Chemistry: Cambridge, UK, 2009.

14. Kralik, M.; Corain, B.; Zecca, M. Catalysis by metal nanoparticles supported on functionalized polymers. *Chem. Pap.* **2000**, *54*, 254–264.

15. Luque, R. *Supported Metal Nanoparticles in Catalysis. Progress in Heterogeneous Catalysis*; Marmaduke, D., Ed.; Novapublishers: San Diego, CA, USA, 2008.

16. Carrillo-Carrion, C.; Cardenas, S.; Simonet, B.M.; Valcarcel, M. Selective quantification of carnitine enantiomers using chiral cysteine-capped CdSe(ZnS) quantum dots. *Anal. Chem.* **2009**, *81*, 4730–4733. [CrossRef] [PubMed]

17. Cai, D.; Mataraza, J.M.; Qin, Z.H.; Huang, Z.P.; Huang, J.Y.; Chiles, T.C.; Carnahan, D.; Kempa, K.; Ren, Z.F. Highly efficient molecular delivery into mammalian cells using carbon nanotube spearing. *Nat. Methods* **2005**, *2*, 449–454. [CrossRef] [PubMed]

18. Campelo, J.M.; Luna, D.; Luque, R.; Marinas, J.M.; Romero, A.A. Sustainable preparation of supported metal nanoparticles and their applications in catalysis. *ChemSusChem* **2009**, *2*, 18–45. [CrossRef] [PubMed]

19. Gedanken, A. Using sonochemistry for the fabrication of nanomaterials. *Ultrason. Sonochem.* **2004**, *11*, 47–55. [CrossRef] [PubMed]

20. Luque, R.; Mariana Balu, A.; Manuel Campelo, J.; Gonzalez-Arellano, C.; Jose Gracia, M.; Luna, D.; Maria Marinas, J.; Angel Romero, A. Tunable shapes in supported metal nanoparticles: From nanoflowers to nanocubes. *Mater. Chem. Phys.* **2009**, *117*, 408–413. [CrossRef]

21. Yoshida, K.; Gonzalez-Arellano, C.; Luque, R.; Gai, P.L. Efficient hydrogenation of carbonyl compounds using low-loaded supported copper nanoparticles under microwave irradiation. *Appl. Catal. A Gen.* **2010**, *379*, 38–44. [CrossRef]

22. Marquez-Medina, M.D.; Prinsen, P.; Li, H.; Shih, K.; Romero, A.A.; Luque, R. Continuous-flow synthesis of supported magnetic iron oxide nanoparticles for efficient isoeugenol conversion into vanillin. *ChemSusChem* **2018**, *11*, 389–396. [CrossRef]

23. Gonzalez-Arellano, C.; Yoshida, K.; Luque, R.; Gai, P.L. Highly active and selective supported iron oxide nanoparticles in microwave-assisted N-alkylations of amines with alcohols. *Green Chem.* **2010**, *12*, 1281–1287. [CrossRef]

24. Saberi, F.; Rodriguez-Padron, D.; Doustkhah, E.; Ostovar, S.; Franco, A.; Shaterian, H.R.; Luque, R. Mechanochemically modified aluminosilicates for efficient oxidation of vanillyl alcohol. *Catal. Commun.* **2019**, *118*, 65–69. [CrossRef]

25. Zheng, Y.; Monty, J.; Linhardt, R.J. Polysaccharide-based nanocomposites and their applications. *Carbohyd. Res.* **2015**, *405*, 23–32. [CrossRef]

26. Quignard, F.; Di Renzo, F.; Guibal, E. From natural polysaccharides to materials for catalysis, adsorption, and remediation. *Top. Curr. Chem.* **2010**, *294*, 165–197. [PubMed]

27. Abdelaal, H.M.; Hardbrecht, B. Template-assisted synthesis of metal oxide hollow spheres utilizing glucose derived-carbonaceous spheres as sacrificial templates. *J. Adv. Chem. Eng.* **2014**, *5*. [CrossRef]

28. Chen, W.; Zhong, L.; Peng, X.; Lin, J.; Sun, R. Xylan-type hemicelluloses supported terpyridine-palladium(II) complex as an efficient and recyclable catalyst for Suzuki-Miyaura reaction. *Cellulose* **2014**, *21*, 125–137. [CrossRef]

29. Dignum, M.J.W.; Kerler, J.; Verpoorte, R. Vanilla production: Technological, chemical, and biosynthetic aspects. *Food Rev. Int.* **2001**, *17*, 199–219. [CrossRef]

30. Adilina, I.B.; Hara, T.; Ichikuni, N.; Shimazu, S. Oxidative cleavage of isoeugenol to vanillin under molecular oxygen catalysed by cobalt porphyrin intercalated into lithium taeniolite clay. *J. Mol. Catal. A Chem.* **2012**, *361*, 72–79. [CrossRef]

31. Zhao, L.Q.; Xie, Y.M.; Chen, L.Y.; Xu, X.F.; Zha, C.X.; Cheng, F. Efficient biotransformation of isoeugenol to vanillin in recombinant strains of Escherichia coli by using engineered isoeugenol monooxygenase and sol-gel chitosan membrane. *Process Biochem.* **2018**, *71*, 76–81. [CrossRef]

32. Immoos, J.E. A novel synthesis of isoeugenol, ring-(U)-C-14. *J. Label. Compd. Radiopharm.* **2015**, *58*, 419–424. [CrossRef]

33. Herrmann, W.A.; Weskamp, T.; Zoller, J.P.; Fischer, R.W. Methyltrioxorhenium: Oxidative cleavage of CC-double bonds and its application in a highly efficient synthesis of vanillin from biological waste. *J. Mol. Catal. A Chem.* **2000**, *153*, 49–52. [CrossRef]

34. Kacurakova, M.; Wellner, N.; Ebringerova, A.; Hromadkova, Z.; Wilson, R.H.; Belton, P.S. Characterisation of xylan-type polysaccharides and associated cell wall components by FT-IR and FT-Raman spectroscopies. *Food Hydrocoll.* **1999**, *13*, 35–41. [CrossRef]

35. Ma, Y.; He, H.; Wu, J.; Wang, C.; Chao, K.; Huang, Q. Assessment of polysaccharides from Mycelia of genus *Ganoderma* by mid-infrared and near-infrared spectroscopy. *Sci. Rep.* **2018**, *8*. [CrossRef]

36. Ikeya, T.; Senna, M. Change in the structure of niobium pentoxide due to mechanical and thermal treatments. *J. Non-Cryst. Solids* **1988**, *105*, 243–250. [CrossRef]

37. Braga, V.S.; Dias, J.A.; Dias, S.C.L.; de Macedo, J.L. Catalyst materials based on $Nb_2O_5$ supported on $SiO_2$-$Al_2O_3$: Preparation and structural characterization. *Chem. Mater.* **2005**, *17*, 690–695. [CrossRef]

38. Xu, C.; Ojeda, M.; Arancon, R.A.D.; Romero, A.A.; Domingo, J.L.; Gomez, M.; Blanco, J.; Luque, R. Bioinspired Porous ZnO Nanomaterials from fungal polysaccharides: Advanced materials with unprecedented low toxicity in vitro for human cells. *ACS Sustain. Chem. Eng.* **2015**, *3*, 2716–2725. [CrossRef]

39. Raba, A.M.; Bautista-Ruiz, J.; Joya, M.R. Synthesis and structural properties of niobium pentoxide powders: A comparative study of the growth process. *Mater. Res. Ibero Am. J.* **2016**, *19*, 1381–1387. [CrossRef]

40. Murayama, T.; Chen, J.; Hirata, J.; Matsumoto, K.; Ueda, W. Hydrothermal synthesis of octahedra-based layered niobium oxide and its catalytic activity as a solid acid. *Catal. Sci. Technol.* **2014**, *4*, 4250–4257. [CrossRef]

41. Wu, J.; Li, J.; Lue, X.; Zhang, L.; Yao, J.; Zhang, F.; Huang, F.; Xu, F. A one-pot method to grow pyrochlore $H_4Nb_2O_7$-octahedron-based photocatalyst. *J. Mater. Chem.* **2010**, *20*, 1942–1946. [CrossRef]

42. Bocca, B.; Sabbioni, E.; Mieti, I.; Alimonti, A.; Petrucci, F. Size and metalcomposition characterization of nano and microparticles in tatto inks by acombination of analytical techniques. *J. Anal. At. Spectrom.* **2017**, *32*, 616–628. [CrossRef]

43. Xu, C.; De, S.; Balu, A.M.; Ojeda, M.; Luque, R. Mechanochemical synthesis of advanced nanomaterials for catalytic applications. *Chem. Commun.* **2015**, *51*, 6698–6713. [CrossRef]

44. Garcia, A.; Alriols, M.G.; Spigno, G.; Labidi, J. Lignin as natural radical scavenger. Effect of the obtaining and purification processes on the antioxidant behaviour of lignin. *Biochem. Eng. J.* **2012**, *67*, 173–185. [CrossRef]

45. Franco, A.; De, S.; Balu, A.M.; Garcia, A.; Luque, R. Mechanochemical synthesis of graphene oxide-supported transition metal catalysts for the oxidation of isoeugenol to vanillin. *Beilstein J. Org. Chem.* **2017**, *13*, 1439–1445. [CrossRef]